Spatial Resolution of Attenuation Imaging

Ziemowit KLIMONDA, Jerzy LITNIEWSKI, Andrzej NOWICKI

Institute of Fundamental Technological Research
Polish Academy of Sciences
Pawińskiego 5B, 02-106 Warszawa, Poland
e-mail: zklim@ippt.gov.pl

The attenuating properties of biological tissue are of great importance in ultrasonic examination even though its anatomical variability limits diagnostics effectiveness. We are currently developing a technique for parametric imaging of attenuation and we intend to apply it for in vivo characterization of tissue. The diagnostic usefulness of the proposed technique crucially depends on the precision of the attenuation estimate and the resolution of the parametric image. These two parameters are highly correlated, since the resolution is reduced whenever averaging is used to minimize the errors introduced by the random character of the backscatter. Here we report on the results of numerical processing of both, simulated and recorded from a tissue-mimicking phantom echoes. We have analyzed the parameters of the estimation technique and examined their influence on the precision of the attenuation estimate and on the parametric image resolution. The optimal selection of attenuation image parameters depending on its intended diagnostic use, was also considered.

Keywords: ultrasound attenuation, spatial resolution, parametric imaging.

1. Introduction

The basic operating principle of modern ultrasonic scanners remains unaltered from their origin. Short, wideband pulses are transmitted through the tissue and the backscattered echoes are being received. The envelope of the echo is subsequently detected. The ultrasonic image consists of many lines; each of them corresponds to echo envelope. The B-scan image reflects the distribution of the tissue reflectivity. The RF echoes contain information about the tissue properties that cannot be assessed with the signal envelope. The attenuation of ultrasound is one of such properties with potentially substantial importance in medical diagnostics. It has been demonstrated that pathological state tissue has different attenuation properties than the healthy one. OOSTERVELD *et al.* have

shown that the slope of attenuation coefficient, combined with statistical parameters of image texture can be used to diagnose the diffuse liver disease [11]. Saijo et al. employed scanning acoustic microscope to measure five types of gastric cancer and indicated different attenuation coefficient and sound speed comparing to normal tissue [14]. Bigelow et al. investigated possibility of the prediction of the premature delivery based on the noninvasive ultrasonic attenuation determination [1]. In various other publications it has been reported that pathological processes can lead to changes in the mean attenuation coefficient that range from several percent for cirrhotic human liver, through dozens percent for fatty human liver [6], or degenerated bovine articular cartilage [8] to over a hundred percent in case of porcine liver HIFU treatment in vivo [16] or two hundred percent for porcine kidney thermal coagulation [15]. These reports motivated us to consider the parametric imaging of the attenuation in medical diagnostic tool. There are two approaches to the estimation of ultrasonic attenuation. The spectral difference technique that is based on a comparison of power spectrum of backscattered signals after propagation through the medium and the spectral shift method that uses the downshift of the pulse mean frequency caused by frequency-depended attenuation. In our approach the mean frequency (MF) is directly evaluated from the backscatter. MF is highly variable due to the random character of the backscattering RF signals [3, 12]. The mean frequency variability results in major errors of the attenuation estimation. This limits the spatial resolution, the precision of the attenuation determination and the potential medical applications. Signal variability can be reduced by averaging over the frequency lines (which decreases the lateral resolution) or increasing the window of the frequency estimator (which decreases the longitudinal resolution). This paper examines and optimizes the strategy of averaging the mean frequency lines in the context of attenuation estimation.

2. Methods

The amplitude A of the ultrasound plane wave propagating in homogenous medium decreases exponentially with the penetration depth due to attenuation:

$$A = A_0 \exp(-\alpha x), \tag{1}$$

where A_0 – initial intensity, α – attenuation coefficient and x – wave path length. The attenuation coefficient α depends on frequency f and in the soft tissue have the form:

$$\alpha(f) = \alpha_1 \left(\frac{f}{f_1} \right)^n, \tag{2}$$

where α_1 is attenuation coefficient for frequency f_1 (in the literature generally $f_1 = 1$ MHz) and n for soft tissue is very close to 1 [9]. The linear relation between attenuation coefficient and the wave frequency is often assumed. When

a short ultrasonic pulse propagates within the homogenous medium the dispersion of the attenuation coefficient results in a shift of the pulse MF. To find estimates of the attenuation from ultrasonic echo signals we assume that the attenuation of tissue increases linearly with frequency and that the backscattered signals have the Gaussian shaped spectrum (Gaussian pulse). With this assumptions the MF shift $(f - f_0)$ is given by [4, 5]

$$f - f_0 = \frac{\alpha \cdot \Delta x \cdot \sigma_0^2}{2},$$ (3)

where f_0 and f are MF before and after propagation respectively, σ_0^2 is the variance of the pulse spectrum, Δx denotes penetrated distance and α is the attenuation coefficient that can be calculated from the Eq. (3) as

$$\alpha = -\frac{2}{\sigma_0^2} \frac{\partial f}{\partial x}.$$ (4)

To determine the MF along the propagation path we have applied the MF correlation estimator (I/Q algorithm used in Doppler technique [10]). The results obtained from the selected amount of adjacent B-scan echo-lines were averaged. Then the overall MF shift trends were calculated using Singular Spectrum Analysis (SSA [2]). The attenuation estimates along the propagation path were calculated from MF trends using Eq. (4).The number of averaging scan lines and the length of the time window applied for frequency determination define the spatial resolution of parametric attenuation imaging. The accuracy of the applied method was verified by calculating standard deviation and the maximal error of the attenuation estimates. We defined the maximal error as

$$\sigma_{\mathrm{max}} = \max(|\alpha_{\mathrm{est}} - \alpha_{\mathrm{theor}}|),$$ (5)

where α_{est} and α_{theor} are the estimated and the assumed attenuation coefficient, respectively.

3. Simulations

The artificial RF lines were generated according to the following scheme. A uniform spatial distribution of scattering centers along the 5 cm path in attenuating medium (0.5 dB/MHz/cm) was assumed. The amplitudes of the scatterers were also uniformly distributed.

The received pulse-echo signal was simulated by superposition of all of the elementary, individually scattered pulses, taking into account the phase differences caused by spatial location of scatterers and the pulse frequency contents modified by attenuation. The average number of scatterers in the sample volume was 60. The 4.44 MHz gaussian interrogating pulse with bandwidth equal 80% at −6 dB level was assumed. The scatterers positions and amplitudes were different

for each simulation. The example of the simulated RF line and the corresponding MF line is presented in Fig. 1.
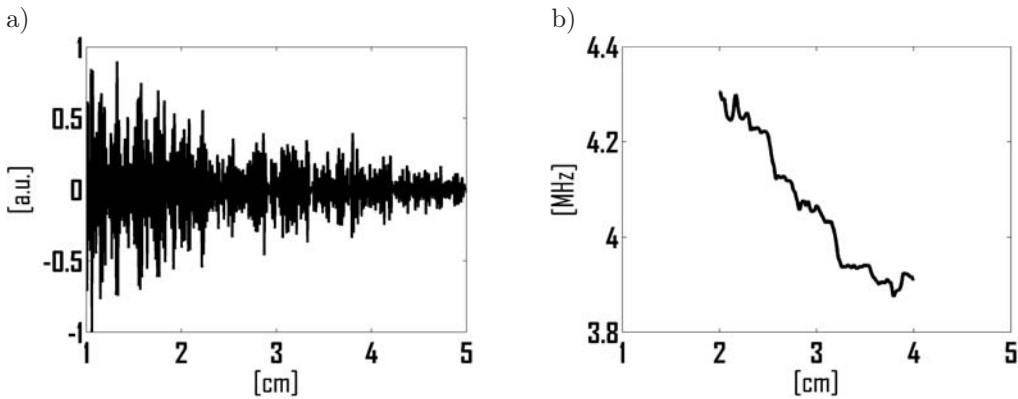
a)

b)

Fig. 1. The simulated RF line (a) and corresponding MF line for IQ window length equal 2 cm (b).

The simulated RF lines were processed according to the scheme presented in Fig. 2. First RF lines were subsequently grouped into 20 packets, each of n lines, with $n \in \{1, 5, 10...50\}$. Then, the following procedure was executed for each packet: first, the MF line was estimated for each line in each packet using selected (1 cm, 2 cm or 3 cm) window length (see chapter 2). Next, the n frequency lines were averaged and the frequency trend was extracted.
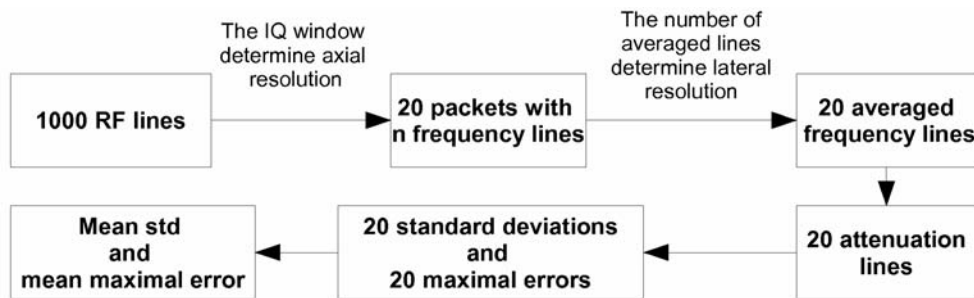

Fig. 2. The simulated RF lines processing scheme.

For each packet the attenuation profile was calculated (Eq. 4) using the estimated frequency trend. Two parameters, standard deviation (SD) and the maximal error (MR) were calculated for each attenuation profile. Thus each packet was associated with parameters that depended on the window size and the averaging. Finally, the mean values and the standard errors of SD and MR were calculated. The results are presented in Fig. 4.

4. Measurements

The RF-echoes from the tissue mimicking phantom (Dansk Phantom Service, model 571, $\alpha = 0.5$ dB/MHz/cm) were recorded. The experimental setup consisted of a flat transducer (15 mm diameter, 5 MHz, 80% 6 dB bandwidth, IMASONIC ME5-1/2", France), a pulser-receiver (Panametric 5900 PR, USA) and a sampling oscilloscope (Agilent Infinium 54810A, USA).

The transducer was moved over the selected area of the phantom with 5 mm steps, and echo data raging from the depth of 1 to 7 cm were collected. 24 scattered waveforms were recorded and processed to calculate attenuation coefficient profiles. The processing was performed for the length of the I/Q algorithm window being equal 1, 2 or 3 cm and the number of averaged lines varying from 1 to 24. The example of measured RF line, corresponding MF line for IQ window length equal 2 cm, the averaged MF line and its trend is presented in Fig. 3.
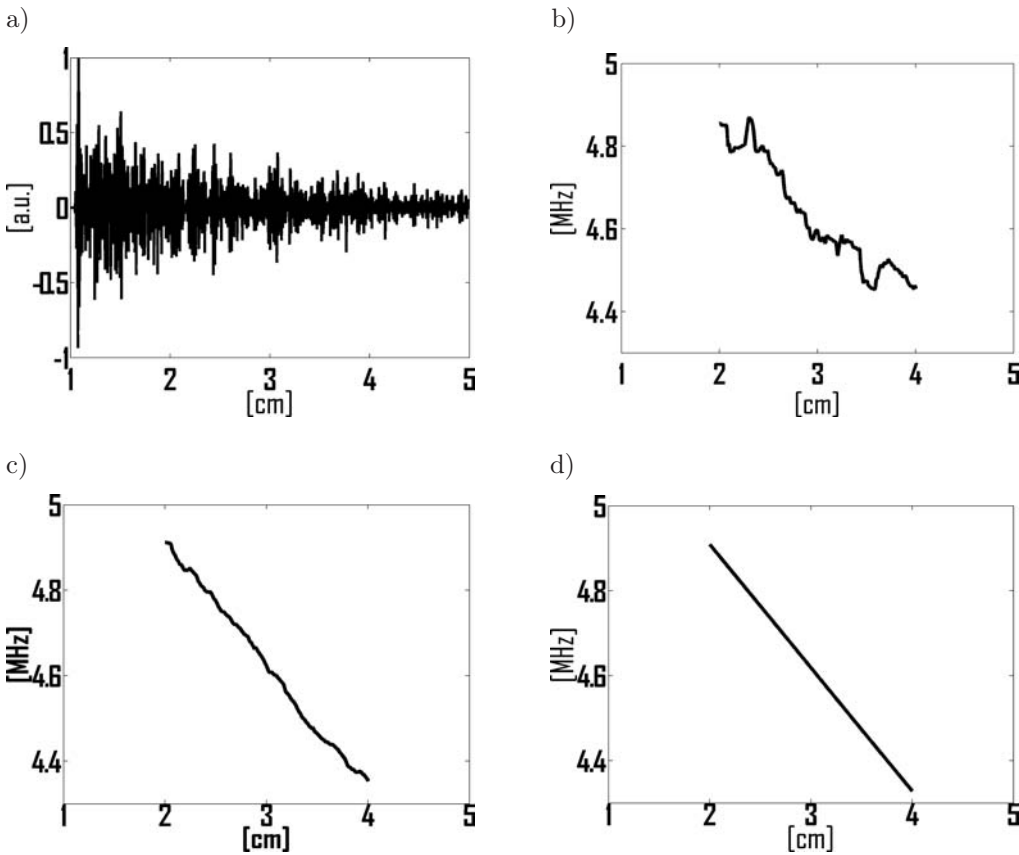

Fig. 3. The measured RF line (a), corresponding MF line for IQ window length equal 2 cm (b), the MF line averaged over 24 measurements (c) and the same line after the SSA trend extraction procedure (d).

Additionally, the B-scan image and corresponding RF data from human liver *in-vivo* were recorded using commercial ultrasonic scanner (Antares, Siemens Medical Solutions USA, Inc.). The scanner was equipped with the 4.44 MHz convex probe and Axius Direct Ultrasound Research Interface which is a dedicated module enabling the recording of raw RF lines. The B-mode image and calculated, corresponding attenuation map is presented in Fig. 6. In processing the IQ window and the number of averaged MF lines was set to 1.5 cm and 30 respectively.

5. Results

However both parameters, the mean SD and mean MR decrease with the number of averaged lines and the IQ window length, the influence of the window is much stronger. For example, by changing the IQ window from 1 cm to 2 cm (Fig. 4) for a constant number of averaged lines being equal to 10, the mean SD decreased from 22.4% to 7.3%. The doubling of the number of averaged lines for a constant 1 cm long IQ window results in lower decrease of the standard deviation (16.5%). Analogous trend is observed for the maximal error – an increase of the IQ window length results in a drop of MR from 46.3% to 17.7%, whereas doubling the number of averaged lines results in a drop to 32.7% only. The IQ window length has therefore significantly greater influence on the quality of the estimation of the attenuation profile than the number of averaged lines.

The experimental data confirms this observation. The results of phantom measurements are presented in Fig. 5. Three attenuation profiles obtained with different window parameters, but all corresponding to a constant scan area (i.e. distance along the Z axis, corresponding to the IQ window multiply by the distance along the X axis, corresponding to the number of averaged lines) are compared. The SD were 15.5%, 11.1% and 7.1% and the MR were 34.2%, 16.8% and 14.3% for profiles corresponding to the IQ windows equal to 1, 2 and 3 cm, respectively. The results of the measurements agree with the simulation, i.e. the measured parameters are within 95% confidence interval for the simulated SD and MR with one exception – the measured SD value for 3 cm window is outside of the 99% confidence interval.

The image of the liver was obtained in vivo and is presented in Fig. 6a together with the calculated attenuation coefficient distribution (Fig. 6b). The spatial resolution in attenuation image can be assumed to be approximately similar to the averaging area equal to 2 cm^2. The attenuation coefficient averaged over the liver tissue was equal to 0.56 ± 0.3 dB/cm·MHz what also corresponds well with published data [6, 7, 13]. Some variation of attenuation within the liver tissue could be of natural reasons as well as could be caused by not satisfactory focusing compensation. Very high attenuation shown at the liver left border (Fig. 6b) could be caused by reflections at the interface.
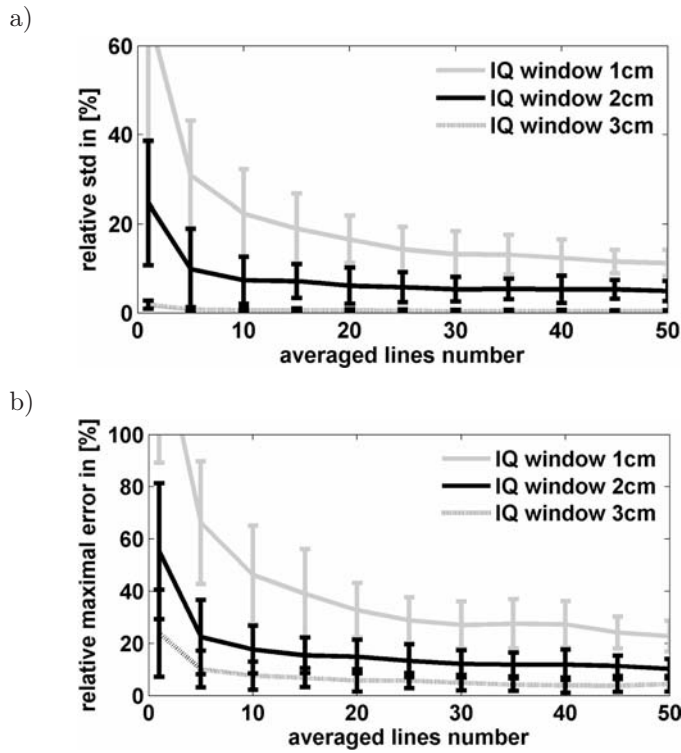
a)

b)

Fig. 4. The simulation results: the standard deviation (a) and the maximal error (b) of the attenuation coefficient vs. the number of averaged lines. The successive lines correspond to IQ windows of 1 cm, 2 cm and 3 cm respectively.
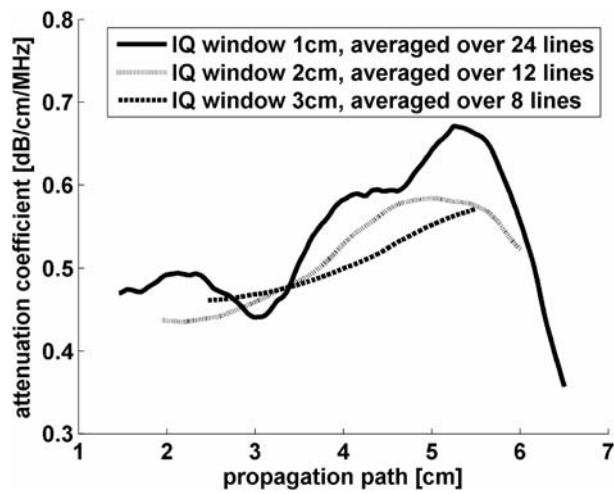

Fig. 5. The measurement results: the attenuation profiles are plotted for different length of IQ window and different number of averaged lines, the averaging area (IQ window length multiply by the number of averaged lines) is constant. The phantom attenuation coefficient was equal 0.5 dB/MHz/cm.
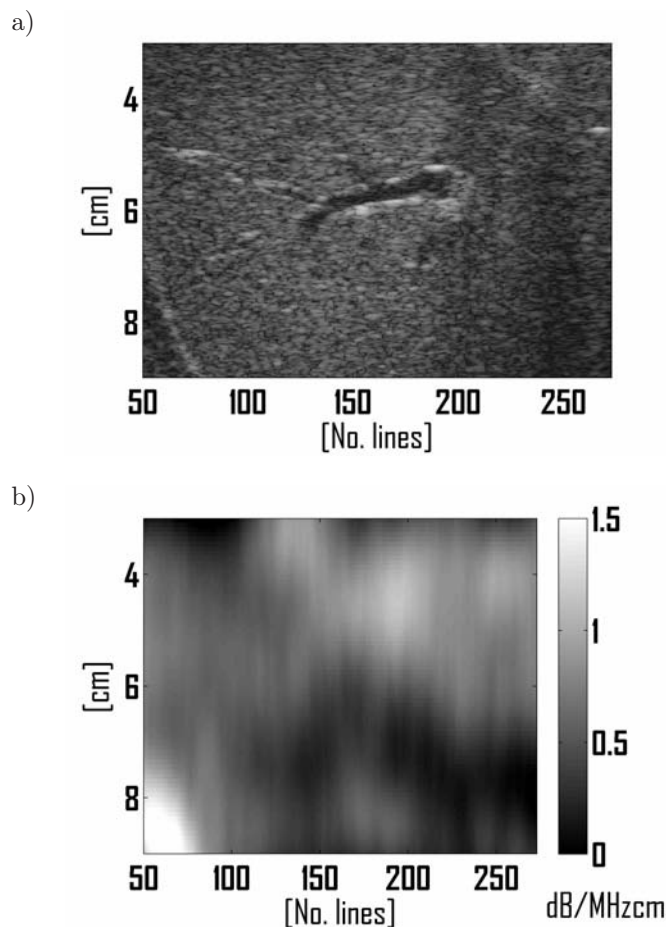
a)

b)

Fig. 6. The B-mode image of the human liver *in-vivo* obtained from commercial scanner (a) and corresponding attenuation map estimated with IQ window length equaled 1.5 cm and averaged MF lines number equaled 30 (b).

6. Conclusions

The results of the simulations and the measurements clearly indicate that the IQ window length stronger influences the accuracy of attenuation estimates than the averaging over the frequency lines. Nevertheless, the averaging of frequency lines is still a useful procedure that significantly improves the precision of the attenuation estimation (see Fig. 4). The simulation results also suggest that the number of averaged lines should not exceed 20–30 as the further increase do not improve very much the attenuation estimates. The parameters of estimation, i.e. the IQ window size and the number of averaged lines, should be selected depending on the application. For example, if we examine the tissue coagulation, we expect large attenuation changes, much larger than 100% [11, 12]. In this case,

the number of averaged lines can be small and the IQ window length can be set to approx. 1 cm. A fatty liver attenuates more than 50% stronger than a healthy liver [6], thus for its examination the number of averaged lines should be above 20 for the IQ window of 1 cm, or just a few lines for 2 cm length of the IQ window. The attenuation of a cirrhotic liver is only a few percent higher than that of a healthy one (it has been reported about 6% [6]). Probably, in this case, the resolution of attenuation estimation is not sufficient for parametric imaging but still it is possibly to obtain valuable results when the averaged attenuation of the liver is considered. For example, processing the simulated RF echoes with the IQ window length of 3 cm, and applying averaging over 50 lines the mean standard deviation and the maximal error are obtained equal to 0.37% and 4.5%, respectively. In this case, low spatial resolution of attenuation estimation is compensated with the high accuracy.

In the paper the parametric image of attenuation coefficient distribution was presented. The frequency dependent attenuation is an interesting acoustic parameter for tissue characterization. Usually, tissue-attenuating properties averaged over large areas are presented. However, it has been shown that imaging is the best diagnostic technique. Conventional ultrasonic imaging as well as other medical visualization methods is successfully applied in all medical fields. Their usefulness is closely connected with physician's experience, not with numerical data that can be extracted from ultrasonic waves or another kind of radiation applied for examination. Thus, it could be anticipated that also parametric attenuation imaging is a promising diagnostic technique.

Acknowledgments

References

[1] BIGELOW T.A., MCFARLIN B.L., O'BRIEN W.D., OELZE M.L., *In vivo ultrasonic attenuation slope estimates for detectiong cervical ripening in rats: Preliminary results*, Journal of Acoustical Society of America, **123**, 3, 1794–1800 (2008).

[2] GOLYANDINA N., NEKRUTKIN V., AHIGLJAVSKY A., *Analysis of time Series Structure: SSA and related techniques*, Chapman & Hall/CRC, 2001.

[3] KLIMONDA Z., NOWICKI A., *Imaging of the mean frequency of the ultrasonic echoes*, Archives of Acoustics, **32**, 4 (Supplement), 77–80 (2007).

[4] LAUGIER P., BERGER G., FINK M., PERRIN J., *Specular reflector noise: effect and correction for in vivo attenuation estimation*, Ultras. Imag., **7**, 277–292 (1985).

[5] Litniewski J., *Assessment of trabecular bone structure deterioration by ultrasound* [in Polish:] *Wykorzystanie fal ultradźwiękowych do oceny zmian struktury kości gąbczastej*, Prace IPPT, 2006.

[6] Lu Z.F., Zagzebski J., Lee F.T., *Ultrasound Backscatter and Attenuation in Human Liver With Diffuse Disease*, Ultrasound in Med. & Biol., **25**, 7, 1047–1054 (1999).

[7] Maklad N., Ophir J., Balsera V., *Attenuation of ultrasound in normal liver and diffuse liver disease in vivo*, Ultras. Imag., **6**, 117–125 (1984).

[8] Nieminen H.J., Saarakkala S., Laasanen M.S., Hirvonen J., Jurvelin J.S., Töyräs J., *Ultrasound Attenuation in Normal and Spontaneously Degenerated Articular Cartilage*, Ultrasound in Med. & Biol., **30**, 4, 493–500 (2004).

[9] Nowicki A., *Ultrasonic Diagnostics* [in Polish:] *Diagnostyka Ultradźwiękowa*, MAKmed, 2000.

[10] Nowicki A., *Fundamentals of Doppler Ultrasonography* [in Polish:] *Podstawy Ultrasonografii Dopplerowskiej*, PWN, 1995.

[11] Oosterveld B.J., Thijssen J.M., Hartman P.C., Romijn R.L., Rosenbusch G.J., *Ultrasound attenuation and texture analysis of diffuse liver disease: methods and preliminary results*, Phys. Med. Biol., **36**, 8, 1039–1064 (1991).

[12] Ophir J., Ghouse M.A., Ferrari L.A., *Attenuation estimation with the zero crossing technique: phantom studies*, Ultras. Imag., **7**, 122–132 (1985).

[13] Parker K.J., Asztely M.S., Lerner R.M., Schenk E.A., Waag R.C., *In-vivo measurements of ultrasound attenuation in normal or diseased liver*, Ultrasound in Med. & Biol., **14**, 2, 127–136 (1988).

[14] Saijo Y., *High Frequency Acoustic Properties of Tumor Tissue* [In:] *Ultrasonic Tissue Characterization*, Springer-Verlag, Tokio 1996.

[15] Worthington A.E., Sherar M.D., *Changes in Ultrasound Properties of Porcine Kidney Tissue During Heating*, Ultrasound in Med. & Biol., **27**, 5, 673–682 (2001).

[16] Zderic V., Keshavarzi A., Andrew A.M., Vaezy S., Martin R.W., *Attenuation of Porcine Tissues In Vivo After High Intensity Ultrasound Treatment*, Ultrasound in Med. & Biol., **30**, 1, 61–66 (2004).